Symmetry protection and giant Fermi arcs from multifold fermions in binary, ternary, and quaternary compounds

Chanchal K. Barman,[1,*] Chiranjit Mondal,[2,*] Sumiran Pujari,[1] Biswarup Pathak,[2,3,†] and Aftab Alam[1,‡]

[1]*Department of Physics, Indian Institute of Technology, Bombay, Powai, Mumbai 400076, India*

[2]*Discipline of Metallurgy Engineering and Materials Science, IIT Indore, Simrol, Indore 453552, India*

[3]*Discipline of Chemistry, School of Basic Sciences, IIT Indore, Simrol, Indore 453552, India*

(Received 29 February 2020; revised 24 July 2020; accepted 2 October 2020; published 30 October 2020)

Higher-fold chiral fermions that go beyond twofold Weyl fermions have recently been reported in crystalline systems. Here, we focus on such excitations in several binary, ternary, and quaternary alloys/compounds with CoGe, BiSbPt, and $KMgBO_3$ as the representative examples that belong to the crystal space group 198. We found distinct threefold, fourfold, and sixfold chiral fermions in the bulk via density-functional computations. We provide general symmetry arguments for the protection of these degeneracies with special emphasis on the fourfold fermions. Our surface spectra simulations show that the size of Fermi arcs resulting from these chiral fermions are large, robust, and untouched from the bulk states due to the near absence of trivial bulk Fermi pockets. All these features make these systems—especially CoGe and $KMgBO_3$—promising topological semimetal candidates to realize higher-fold fermions in future photoemission and transport experiments.

DOI: 10.1103/PhysRevB.102.155147

I. INTRODUCTION

The discovery of chiral fermions in solid-state quantum materials has kick-started a burst of activity in condensed-matter physics. A methodological approach toward the understanding and search for new topological semimetals is to examine how the symmetries of a material enforce or symmetry protect degenerate multifold band-crossing points [1,2]. These new quasiparticles [3–6] in the solid state [7–17] may not even have elementary particle counterparts.

Some of the new, unexpected quasiparticle excitations predicted recently are spin-1 [15–18], charge-2 Dirac [17,18], and spin-$\frac{3}{2}$ [17] chiral fermions. The well-known twofold Weyl chiral fermions can be present in the absence of either inversion ($\mathcal{I}$) or time reversal ($\mathcal{T}$) symmetry in three-dimensional (3D) crystals. They are characterized by nonzero topological charges called Chern numbers (C $= \pm 1$) [5,6]. These Weyl fermions can be described by an effective spin-$\frac{1}{2}$ Hamiltonian $H \propto \hbar\, \delta\vec{\mathbf{k}} \cdot \vec{\sigma}$ at lowest order. $\delta\vec{\mathbf{k}}$ is small deviations from the Weyl node in momentum space. $\vec{\sigma} \equiv \{\sigma_x, \sigma_y, \sigma_z\}$ are the 2×2 Pauli matrices. However, certain crystal symmetries can also protect spin-1 or spin-$\frac{3}{2}$ chiral fermions [17,18] at high-symmetry points in the crystal momentum space. They are threefold and fourfold, respectively. Their effective low-energy Hamiltonians are $H \propto \hbar\, \delta\vec{\mathbf{k}} \cdot \vec{\mathbf{L}}$, where L_i's are (3×3) spin-1 and (4×4) spin-$\frac{3}{2}$ rotation generators, respectively. The low-energy dispersions of these multi-Weyl systems follow from the corresponding model Hamiltonians, e.g., spin-1 fermions possess a combination of a Dirac-type linear band crossing and a flat band, as shown in Fig. 1(a), with C $= \pm 2$ and 0, respectively.

Additionally, two identical copies of spin-$\frac{1}{2}$ Weyl nodes can also be symmetry protected [16,18]. This leads to $C = \pm 2$ with fourfold degeneracy. The effective Hamiltonian for such a multi-Weyl node [16,18] can be described as $H \propto \hbar\, \delta\vec{\mathbf{k}} \cdot \vec{\sigma} \otimes \mathbb{I}_{2\times 2}$. They have been named charge-2 Dirac nodes. Figure 1(a) shows schematic diagrams of low-energy dispersions for Dirac, Weyl, spin-1, and charge-2 Dirac nodes. The symmetry-protected band crossings which carry C $= \pm 2$ are referred to as double Weyl nodes. These band crossings are topologically robust under infinitesimal changes of the Hamiltonian parameters [19] and lead to quite interesting phenomena [6].

In the search for such multi-Weyl systems, there have been a few studies on binary transition - silicides with space group (SG) 198, which are predicted to be double Weyl semimetals [15–18,20–23]. Here, we study several binary, ternary, and quaternary alloys with CoGe, BiSbPt, and $KMgBO_3$ as the representative case, respectively. We provide a detailed analysis including *ab initio* simulations of bulk and surface excitations and symmetry-protection arguments for various multifold degeneracies. Unlike previous reports which were geared toward binary systems, our symmetry arguments are quite general in the spirit of Kramers theorem and are independent of the composition of the constituent elements. We performed *ab initio* electronic structure calculations using VIENNA AB INITIO SIMULATION PACKAGE [24,25] with Perdew-Burke-Ernzerhof [25] exchange correlation. Chern numbers were calculated using Wannier charge center evolution of maximally localized Wannier functions [26–28] from WANNIER90 [29]. Surface spectra and Fermi arcs (FAs) were simulated using iterative Green's function method [30–32]. Further information on

*These authors contributed equally to this work.

†biswarup@iiti.ac.in

‡aftab@iitb.ac.in

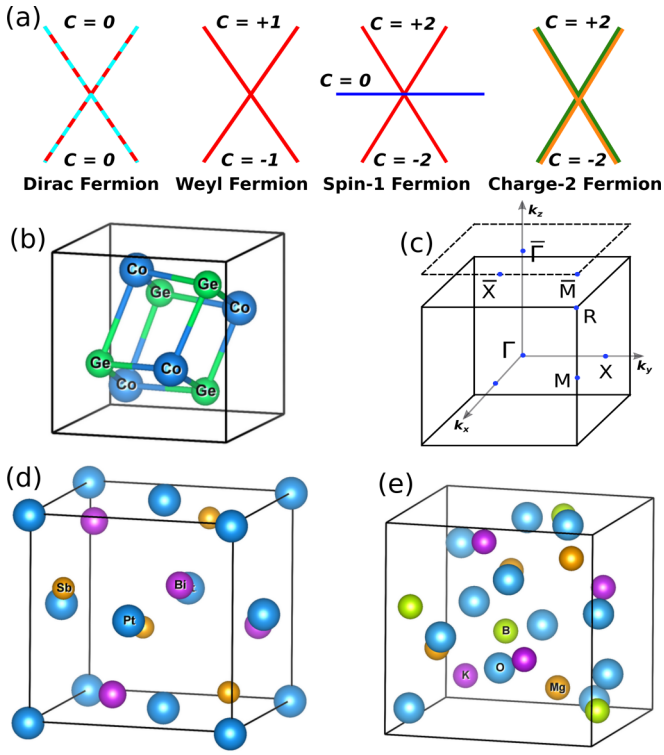

FIG. 1. (a) Schematic band structure of Dirac, Weyl, spin-1, and charge-2 fermions. (b) Crystal structure of CoGe (space group $P2_13$). (c) Bulk Brillouin zone (BZ) and (001) surface BZ (represented by dashed square). Crystal structure of (d) ternary BiSbPt and (e) quaternary $KMgBO_3$.

computational details can be found in the Supplemental Material (SM) [33].

II. CRYSTAL STRUCTURES

The crystal structure and the corresponding Brillouin zone (BZ) for CoGe are shown in Figs. 1(b) and 1(c). CoGe crystallizes in cubic structure with SG $P2_13$ under high pressure [34,35]. The primitive cell contains four formula units with both Co and Ge atoms lying on threefold axes occupying the same Wyckoff sites $4a$ (x, x, x). The internal co-ordinates are $x_{\mathrm{Co}} = 0.1359$ and $x_{\mathrm{Ge}} = 0.8393$. The theoretically optimized lattice parameter of CoGe is found to be 4.64 Å, which matches fairly well with the experimental value, 4.637 Å [34].

Figures 1(d) and 1(e) show the crystal structure of BiSbPt and $KMgBO_3$ compounds. Similar to binary CoGe, the primitive cell of ternary BiSbPt contains four formula units with Bi, Sb, and Pt occupying $4a(x, x, x)$ Wyckoff sites where $x_{\mathrm{Bi}} = 0.629$, $x_{\mathrm{Sb}} = 0.373$ and $x_{\mathrm{Pt}} = 0.990$. The optimized lattice parameter for BiSbPt is found to be 6.69 Å. In $KMgBO_3$, the K, Mg, and B atoms are located in one crystallographic position $4a(x, x, x)$, while the O atoms sit on a different Wyckoff site $12b(y^1, y^2, y^3)$, where $x_{\mathrm{K}} = 0.1333$, $x_{\mathrm{Mg}} = 0.8552$, $x_{\mathrm{B}} = 0.4076$, $y^1_{\mathrm{O}} = 0.4181$, $y^2_O = 0.2572$, and $y^3_O = 0.5405$. The optimized lattice parameter for $KMgBO_3$ is found to be 6.89 Å, which is in fair agreement with the experimental value 6.83451 Å [36].

III. SYMMETRY ARGUMENTS

The crystal structure of these systems has tetrahedral (T_4) point-group symmetry with the following information germane to our analysis [37]. The point group has three generators at Γ point: two screws, $S_{2z} = \{C_{2z}|\frac{1}{2}, 0, \frac{1}{2}\}$, $S_{2y} = \{C_{2y}|0, \frac{1}{2}, \frac{1}{2}\}$ and a threefold rotation $S_3 = \{C^+_{3,111}|0, 0, 0\}$. They satisfy $S_{2z}S_3 = S_3S_{2y}$ and $S_3S_{2z}S_{2y} = S_{2y}S_3$. Due to S_3, the third screw symmetry $S_{2x} = \{C_{2x}|\frac{1}{2}, \frac{1}{2}, 0\}$ is also present. On the other hand, at the R point, the three generators are $S_{2x} = \{C_{2x}|\frac{1}{2}, \frac{3}{2}, 0\}$, $S_{2y} = \{C_{2y}|0, \frac{3}{2}, \frac{1}{2}\}$, and $S_3 = \{C^{-1}_{3,111}|0, 1, 0\}$. They satisfy $S_{2x}S_3 = S_3S_{2y}$ and $S_3S_{2x}S_{2y} = S_{2y}S_3$. We also keep time-reversal symmetry and thus will focus on the time-reversal invariant momenta in the BZ.

We start with the spinless case for which time-reversal operator ($\mathcal{T}$) squares to identity ($\mathbb{I}$). This case is relevant for systems composed of light elements with weak spin-orbit coupling (e.g., $KMgBO_3$), as well as for phonon spectra [18] for this crystal structure. At the Γ point, the electronic structure can potentially show a threefold band degeneracy. However, the Γ point symmetries do not necessarily imply threefold degeneracies. For a threefold degeneracy, the two screw symmetries S_{2y} and S_{2z} should *commute* and square to $\mathbb{I}$ as is the case at Γ, as well as S_3 should act nontrivially ($S_3|\psi\rangle \neq |\psi\rangle$ where $|\psi\rangle$ is a simultaneous eigenstate of S_{2y} and S_{2z}; see supplementary Sec. I.C of Ref. [3]. It turns out that there can also be twofold degeneracies or onefold states at the Γ point consistent with the symmetries if S_3 is trivial.

The symmetry properties at the R point are crucially different. At this point, the two screws S_{2x} and S_{2y} now *anticommute* and square to $-\mathbb{I}$, and hence the previous threefold degeneracy argument does not apply anymore. Reference [18] offered an intuition that the degeneracy at the R point has to be even-dimensional with a lower bound of four [38]. From our analysis, we shall show that it has to be even with an upper bound of four in the presence of S_3.

First, we can get a twofold degeneracy using the anticommutation of the screws: $|\psi\rangle$ and $S_{2x}|\psi\rangle$ are distinct eigenstates under S_{2y}, say with eigenvalues of i and $-i$, respectively, without loss of generality. We can get a further twofold degeneracy due to $S_{2z}S_3 = S_3S_{2y}$: $S_3|\psi\rangle$ and $S_{2y}S_3|\psi\rangle$ are distinct eigenstates now under S_{2x} with eigenvalues i and $-i$, respectively. If S_3 is nontrivial [39] and takes us out of the subspace of $|\psi\rangle$ and $S_{2x}|\psi\rangle$, i.e., minimally $\langle\psi|S_3\psi\rangle = 0$, then mutual orthogonality of the two pairs is ensured [40]. Time reversal (effectively complex conjugation) does not generate any new states for spinless electrons. Since we have accounted for all the symmetries present at R, we can at most get a symmetry-protected fourfold degeneracy and *no higher*. Combining with the argument of Ref. [18], we arrive at an *exactly* fourfold node protected by symmetries.

Going to the spinfull case for which $\mathcal{T}^2 = -\mathbb{I}$, the Kramers degeneracies are lifted throughout the zone except at the time-reversal invariant momenta in the presence of spin-orbit interaction (SOI) because the crystal does not possess space-inversion symmetry. Adding the spin quantum number to a potential threefold spinless degeneracy at Γ, we would like to understand what happens to the six states under SOI. It turns out that they cannot give rise to a sixfold degeneracy, but at least have to split into two nodal points with fourfold

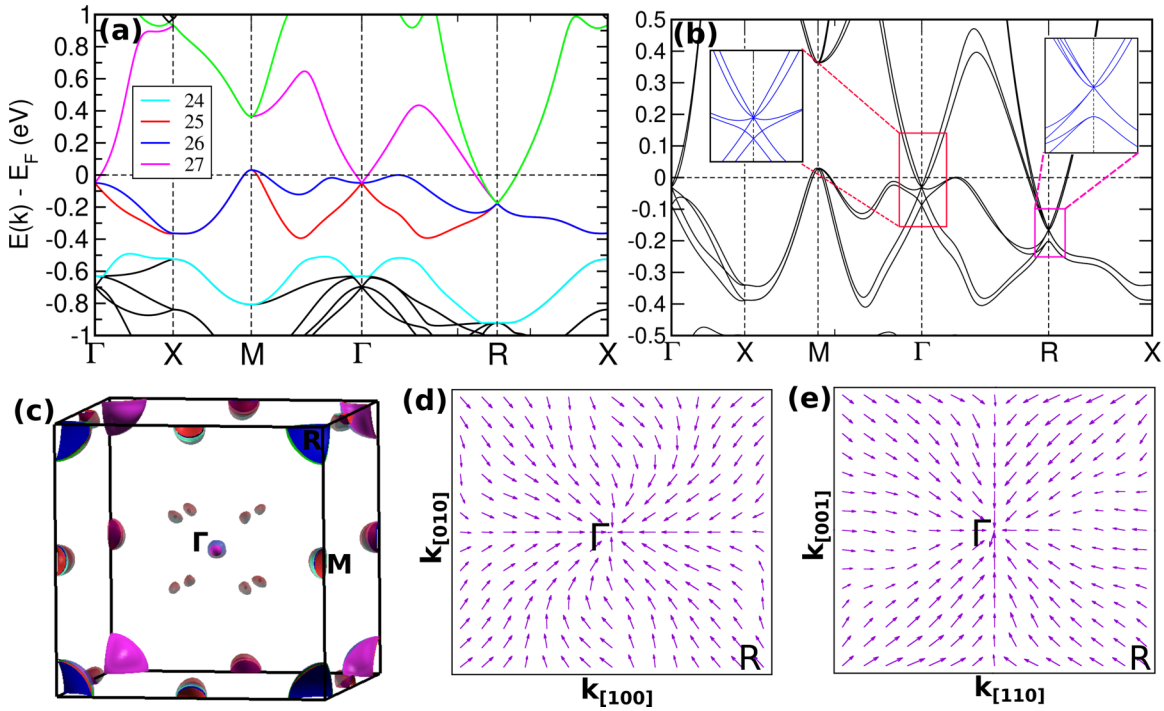

FIG. 2. (a), (b) Band structure of CoGe without (left) and with (right) spin-orbit interaction (SOI). The various degeneracies at the nodal points are protected by nonsymmorphic screw and threefold rotation symmetries of SG 198 and time-reversal symmetry. (c) 3D Fermi surface at isolevel E_F with SOI. (d), (e) In-plane Berry curvature plotted on $k_z = 0$ (left) and $k_x = k_y$ (right) plane, highlighting its flows between R and Γ points in agreement with the sign of the topological charges in the presence of SOI.

degenerate and twofold degenerate states. This is because only a fourfold degeneracy can at most be protected by Γ point symmetries. The reason for this is that now the screws S_{2y} and S_{2z} anticommute (and square to $-\mathbb{I}$) at the Γ point instead of the R point for the spinless case [41]. So, we can again get a fourfold degeneracy by the argument previously made for the spinless case at R point. However, for the spinfull case, time reversal could potentially generate new eigenstates. But, *mutual* orthogonality of S_{2y} and S_{2z} eigenstates and their time-reversed partners is *not* ensured due to imaginary eigenvalues under the screws [40]. Thus, we can only conclude a fourfold degeneracy and no higher. This completes the splitting argument. Also, a singlefold spinless band at Γ (if S_3 is trivial) will give rise to Kramers twofold degeneracy in the spinfull case. Similarly, a fourfold spinfull degeneracy arising from a twofold spinless degeneracy is also consistent with the symmetries. On the other hand, at R point there can be sixfold degeneracies [3].

To explain the spinfull fourfold degeneracy at the Γ point for binary systems, an alternate top-down argument was given in Ref. [15]. Chang *et al.* started with an eight-dimensional representation of the Hamiltonian after making (minimal) assumptions on the nature of the orbitals in the unit cell. They then wrote down the distinct symmetry allowed "mass" terms in the $\mathbf{k} \cdot \mathbf{p}$ Hamiltonian based on the procedure laid down in Ref. [42] to reduce down to a fourfold degeneracy. Our arguments [40] above are rather bottom up and purely based on symmetries of the SG. On the other hand, comparing with the arguments of Ref. [3] for the case of commuting screws, we have paid attention to the interplay of S_3 symmetry of SG 198 with anticommuting screws, which forbids any degeneracies higher than fourfold (and *only* fourfold for the spinless case at the R point). In particular, our arguments also predict that systems beyond the binary class, e.g., ternaries and quaternaries in SG 198 will also host these fourfold degeneracies.

We finally note that the fourfold degeneracies at the R point have charge-2 Dirac nodal character. This is ensured because of the presence of twofold line degeneracies along R-X and M-X directions (in fact, the whole $k_x = \pi$ and symmetry-related planes). Such additional symmetry protection is obtained from a product of time-reversal and screw symmetries (e.g., $\mathcal{T}S_{2x}$) [40], leading to Kramers-like twofold degeneracies. Fourfold degeneracies at the Γ point are not so constrained and therefore generically have spin-$\frac{3}{2}$ character instead.

IV. RESULTS AND DISCUSSION

A. Binary compound (CoGe)

1. Bulk excitations

In Fig. 2(a), we briefly look at the spinless electronic band structure of CoGe by suppressing SOI. Different colored lines in Fig. 2(a) indicate band index (24 to 27). At Γ, we see a threefold or spin-1 degeneracy as discussed earlier. There are also twofold degeneracies and onefold states at Γ at other energies (not highlighted). The computed Chern number for the 25th–27th bands at the Γ point are found to be $C(25) = -2$, $C(26) = 0$, and $C(27) = +2$, respectively. On the other hand, at the R point, we find *only* fourfold degeneracies in line with the symmetry arguments. One such fourfold degeneracy with charge-2 nodal is highlighted in Fig. 2(a). The computed

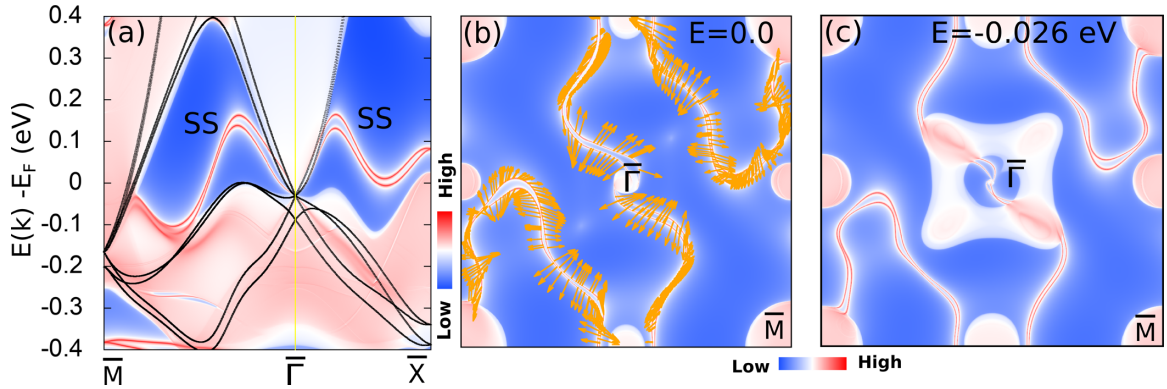

FIG. 3. (a) Surface spectrum of CoGe at (001) surface in presence of SOI. Surface states are marked by SS. Superimposed bulk band structure along R-Γ-X are represented by black lines. (b), (c) Fermi arc contour at E_F and $E_F - 0.026$ eV (spin-3/2 Weyl node). (b) also shows the spin-momentum locked spin texture (orange arrows).

Chern number at this fourfold degenerate node is +2. Hence, the total Chern number is zero in the entire zone in accordance with the Nielsen-Ninomiya theorem [43]. These observations are also pertinent to the weak-SOI case of $KMgBO_3$ to be discussed later [Fig. 5(a)].

The effect of SOI is expected to be relevant for CoGe and BiSbPt, and the corresponding spinfull results are shown in the rest of Figs. 2 and 4(a). At Γ, we get at most a fourfold degeneracy as dictated by symmetry arguments. One such fourfold degeneracy is highlighted in Fig. 2(b). Whereas at the R point, sixfold degeneracy is also allowed by symmetries as highlighted in Fig. 2(b). Figure 2(c) illustrates the Fermi surface (FS) map with SOI. At the Γ point, two concentric spherical shape FSs are found, which arise from the fourfold spin-3/2 excitations. The bands in the inner (outer) sphere possess Chern number $-1(-3)$. At R, FS corresponds to four electronlike bands from double spin-1 excitations with C = +2. Along the Γ-R and at the M point in the BZ, tiny Fermi pockets are observed. We further show the Berry curvature ($\vec{\Omega}$) on $k_z = 0$ and $k_x = k_y$ planes in Figs. 2(d) and 2(e) to highlight that it flows between R and Γ points in agreement with the sign of the topological charges. Notably, under ambient conditions, CoGe crystallizes in the SG $C2/m$ [35,44], where none of the above band topology is observed in our calculations [33].

2. *Surface excitations*

Figure 3 shows the surface state results for these unconventional fermions. FAs on the surface, if present, are generally expected to connect topological nodes of opposite chirality. We studied the (001) surface in which R and Γ points fall at different locations [as shown in Fig. 1(c)] as opposed to the (111) surface to allow for large FAs. In the presence of SOI and consequent doubling of the Chern number ($|C| = 4$) at R and Γ points, there are two pairs of FA states that emerge from the bulk projected states at $\bar{\Gamma}$ and $\bar{M}$ points, as seen from the surface spectrum shown in Fig. 3(a). FA spectral weights are shown in Figs. 3(b) and 3(c) at two different energy cuts. Figure 3(b) also reveals the spin-momentum-locked spin texture of the FAs in the presence of SOI. Without SOI, two doubly spin-degenerate FAs are present (see SM [33] for more details). SOI lifts the spin degeneracy everywhere except at time-reversal invariant momenta, and thus two pairs of FAs appear with antiparallel spin polarization. Such spin-polarized textures may offer applications in spintronics [45,46].

B. Beyond binary compounds

We now report the simulated results of prototype ternary and quaternary systems—BiSbPt and $KMgBO_3$—that belong to the same SG as the binary CoGe. Figure 4(a) displays the bulk band structure of BiSbPt in the presence of SOI. As expected, it shows various higher-fold fermions in concurrence with our general symmetry arguments. Figure 4(b) shows the surface states (SSs) on (001) surface originating from these fourfold and sixfold Weyl nodes in bulk. BiSbPt hosts four pairs of surface states near E_F [shown as SS1 and SS2 in Fig. 4(b)]. SS1 states emerge from the spin-3/2 node just above the E_F, while the SS2 states emerge from the spin-3/2 node at around −0.26 eV below the E_F [see Fig. 4(a)]. In contrast to Ref. [15], where only bulk properties of few ternary compounds are shown, the multifold degenerate Weyl nodes in our predicted BiSbPt compound lie almost at the Fermi level and the extra trivial Fermi pockets are nearly absent. This, in turn, yields clean surface states near E_F [see Fig. 4(b)], however, there are comparatively more spectral weights arising from the bulk than CoGe.

Remarkably, we found that the quaternary compound $KMgBO_3$ from the orthoborate family shows the cleanest FAs when compared to all the systems we studied as well as CoSi from the previous report. $KMgBO_3$ has already been synthe-

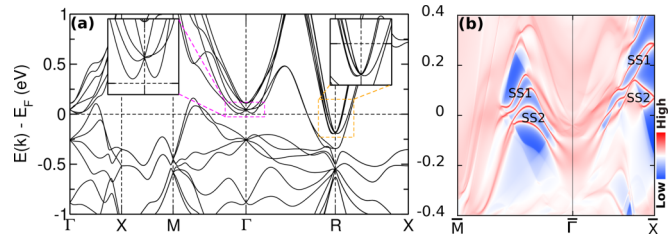

FIG. 4. For BiSbPt with SOI: (a) Electronic band structure and (b) surface spectrum at (001) surface. Surface states are marked by SS. Inset in (a) shows the zoomed view of higher Chern number assisted Weyl nodes at Γ and R points in the BZ.

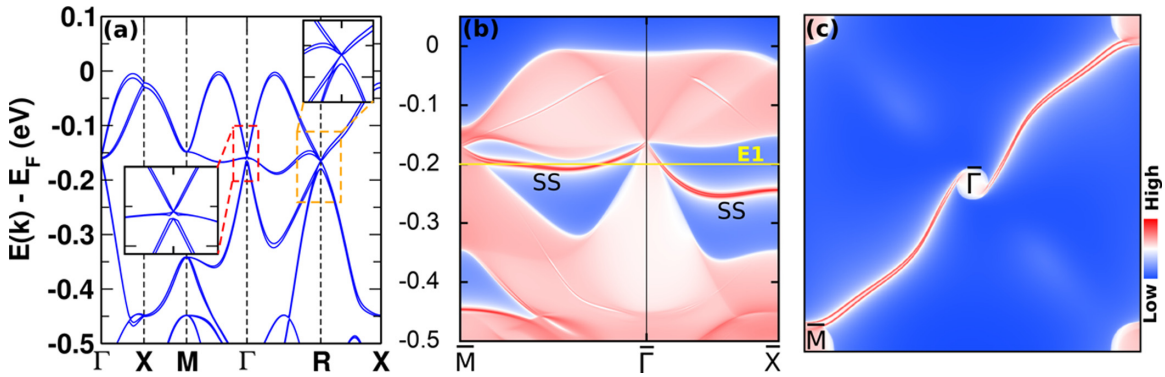

FIG. 5. For $KMgBO_3$ with SOI: (a) Bulk band structure, (b) surface spectrum at side surface (001). Surface states are marked by SS. (c) Fermi arc contour at energy $E1{=}E_F - 0.2$ eV, shown by the horizontal yellow line in (b). As mentioned in the text, SOI-induced splitting is close to imperceptible (compare with Fig. S5 of SM [33]).

sized using solid-state reaction techniques without requiring high pressure [36]. It is expected to have weak SOI because of its light constituent elements. Figure 5 shows the bulk band structure and surface spectra with SOI. As clearly visible, there is a pair of almost degenerate large FAs running from $\bar{\Gamma}$ to $\bar{M}$ with almost no mixing from the bulk states, thus making $KMgBO_3$ an exciting candidate for future experimental studies. The weak-SOI nature of $KMgBO_3$ is corroborated by the negligible effect of SOI on both the bulk and surface electronic structures. The maximal SOI-induced splitting is less than 0.01 eV, and the bulk and surface electronic structures is essentially a "doubled copy" of the corresponding spinless band structure (see Fig. S5 of the SM [33]). We note here that SOI effects are already very small for CoSi [20–22] and this should carry over for $KMgBO_3$ as well. The degeneracies in the bulk are again in accordance with earlier symmetry considerations, and can essentially be understood using the spinless arguments. Moreover, we also found several other experimentally synthesized quaternaries [$Ag_4Te(NO_3)_2$, $Ag_4Te(ClO_3)_2$ and Ag_4TeSO_4] with SG 198 and they again show three-, four-, and sixfold degenerate Weyl nodes at Γ and R points in the BZ. The multi-Weyl nodes in these quaternary systems also lie quite close to E_F (see Fig. S6 of the SM) [33].

V. CONCLUSION

It is important to note that the Weyl nodes that appear in systems such as WTe_2 [5], $MoTe_2$ [47], LiAlGe [48], TaAs(P) [49], NbAs(P) [50] and so on are accidental band crossings with the FAs relatively smaller in size. In contrast, the Γ- and *R*-point band crossings in CoGe, BiSbPt, and $KMgBO_3$ (all belonging to SG 198) are robustly protected by the crystal SG symmetries. Also, the FAs on the (001) surface are much larger since the nodes are maximally separated in BZ. Another promising feature of these systems—especially CoGe and $KMgBO_3$—is the "clean" nature of FAs because of the near absence of spectral weights from bulk states at E_F as evident from Figs. 3–5. This makes them relatively superior to many other reported binary alloys (of SG 198), such as GaPt [51], GaPd [52], AlPd [15], AlPt [15,23], RhGe [15], AuBe [53], and *M*Si (M = Fe, Mn, Ru, Re) [18], which suffer from large spectral weight contributions of extra bulk band crossings across E_F. Very recently, experiments [20–22] have borne out these advantages for the related compound CoSi [17], which makes the case for experiments on CoGe and $KMgBO_3$ attractive since they have already been successfully synthesized [34,36].

In summary, we predict an ideal higher Chern-number topological semimetal in CoGe in agreement with previous bulk studies on binary systems with SG 198. We showed giant FA states in this system without much contamination from the bulk states. Furthermore, we have identified the existence of four- and sixfold degenerate Weyl nodes and their novel surface signatures in a ternary BiSbPt and a quaternary compound $KMgBO_3$. These unconventional multi-Weyl nodes lie close to the Fermi level, which make these *beyond binary sytems* experimentally quite promising as well. $KMgBO_3$ additionally has exceptionally clean, giant FA states compared to all other systems as has been emphasized before. At a theoretical level, we gave new, alternate Kramers-theoremlike arguments based on the inter-relationships between two nonsymmorphic screws and threefold rotations of SG 198 to explain the fourfold degeneracies at *R* point for the spinless case (only possibility) and at Γ point for the spinfull case. Thus, they were expectedly seen in all the nonbinary and binary systems with SG 198 that we studied. The energy offset observed between the multi-Weyl nodes at Γ and R points makes these systems suitable for observing quantized circular photogalvanic effects with possibilities for technological applications [15,54]. All these features of CoGe, BiSbPt, and $KMgBO_3$ serve as strong motivation for future experimental investigations to study these candidate chiral semimetals with topological charges larger than $C = \pm 1$.

ACKNOWLEDGMENTS

C.K.B. acknowledges IIT Bombay for financial support in the form of teaching assistantship. C.M. acknowledges MHRD-India for financial support. A.A. acknowledges DST-SERB (Grant No. CRG/2019/002050) for funding to support this research. S.P. acknowledges financial support from

IRCC, IIT Bombay (17IRCCSG011), and SERB, DST, India (SRG/2019/001419).

APPENDIX: DERIVATIONS OF BAND DEGENERACIES AND FURTHER DETAILS ON SYMMETRY ARGUMENTS

This Appendix contains auxiliary elaborations on the symmetry arguments presented concisely in the main text. Section 1 sets up the preliminaries of symmetry operations. Section 2 is devoted to the band degeneracies at Γ and R points for the spinless case. Section 3 is devoted to the analysis of degeneracy for the spinfull case. Section 4 explains the twofold line degeneracies along R-X and M-X high-symmetry directions in the BZ.

1. Some preliminaries

Following usual conventions, we will specify any crystal symmetry operation by a point group operation $\mathcal{O}$ followed by a translation, $\vec{t}$. For pure point group operations, $\vec{t} = (0, 0, 0)$. The rules of combining two crystal symmetry operations are

$$\{\mathcal{O}_1|\vec{t}_1\}\{\mathcal{O}_2|\vec{t}_2\} = \{\mathcal{O}_1\mathcal{O}_2|\mathcal{O}_1\vec{t}_2 + \vec{t}_1\},$$
$$\{\mathcal{O}|\vec{t}\}^{-1} = \{\mathcal{O}^{-1}| - \mathcal{O}^{-1}\vec{t}\}.$$

Pure translations are indicated by $\{\mathbb{I}|\vec{t}\} = e^{-i\vec{k}.\vec{t}}$, where $\mathbb{I}$ is an identity operation, and $\vec{k}$ and $\vec{t}$ are reciprocal wave vector and translation vectors, respectively. We use $\mathcal{R}$ to signify a 2π rotation, which equals $\mathbb{I}$ and $-\mathbb{I}$ for spinless and spinfull cases, respectively.

The twofold (C_2) and threefold (C_3) rotation operators transform lattice coordinates as follows:

$$C_{2x}(x, y, z) \longrightarrow (x, -y, -z),$$
$$C_{2y}(x, y, z) \longrightarrow (-x, y, -z),$$
$$C_{2z}(x, y, z) \longrightarrow (-x, -y, z),$$
$$C_{3,111}(x, y, z) \longrightarrow (z, x, y),$$
$$C^{-1}_{3,111}(x, y, z) \longrightarrow (y, z, x).$$

The matrix representations of these rotation operators are thus as follows:

$$C_{2x} = \begin{pmatrix} 1 & 0 & 0 \\ 0 & -1 & 0 \\ 0 & 0 & -1 \end{pmatrix}; \quad C_{2y} = \begin{pmatrix} -1 & 0 & 0 \\ 0 & 1 & 0 \\ 0 & 0 & -1 \end{pmatrix},$$
$$C_{2z} = \begin{pmatrix} -1 & 0 & 0 \\ 0 & -1 & 0 \\ 0 & 0 & 1 \end{pmatrix}; \quad C_{3,111} = \begin{pmatrix} 0 & 0 & 1 \\ 1 & 0 & 0 \\ 0 & 1 & 0 \end{pmatrix},$$

and we can use them to multiply rotation operators ($\{\mathcal{O}_1\mathcal{O}_2\mathcal{O}_3...\}$) to obtain the net point-group operation. The sum of two translation vectors follows the usual rule:

$$(x_1, y_1, z_1) + (x_2, y_2, z_2) \longrightarrow (x_1 + x_2, y_1 + y_2, z_1 + z_2).$$

Furthermore, the color scheme set up above will be used in the remaining text when needed to allow for easy parsing of the various algebraic manipulations. In some algebraic manipulations, any expression with a given color in any line is replaced in the following line by the right-hand side of the corresponding colored formula above.

2. Spinless case

a. Γ *point*

The little group at the Γ point has $S_{2z} = \{C_{2z}|\frac{1}{2}, 0, \frac{1}{2}\}$, $S_{2y} = \{C_{2y}|0, \frac{1}{2}, \frac{1}{2}\}$ & $S_3 = \{C_{3,111}|0, 0, 0\}$ as the symmetry generators [37]. These generators satisfy the following relations:

$$\begin{aligned} S^2_{2z} &= \left\{C_{2z}|\frac{1}{2}, 0, \frac{1}{2}\right\}\left\{C_{2z}|\frac{1}{2}, 0, \frac{1}{2}\right\} \\ &= \left\{C^2_{2z}|C_{2z}\left(\frac{1}{2}, 0, \frac{1}{2}\right) + \left(\frac{1}{2}, 0, \frac{1}{2}\right)\right\} \\ &= \left\{C^2_{2z}|\left(\frac{\bar{1}}{2}, 0, \frac{1}{2}\right) + \left(\frac{1}{2}, 0, \frac{1}{2}\right)\right\} \\ &= \left\{C^2_{2z}|0, 0, 1\right\} = \{\mathcal{R}|0, 0, 1\} \\ &= \{\mathbb{I}|0, 0, 1\} = 1. \end{aligned} \tag{A1}$$

From now on, we will skip the derivations of the various relations satisfied by the crystal symmetries and only focus on the details of the symmetry protection of the degeneracies. All derivations of crystal symmetry relations are compiled in Sec. VII of the SM [33]. Similar to Eqs. (A1), we also get

$$S^2_{2y} = 1, \tag{A2}$$

$$S^3_3 = 1. \tag{A3}$$

The twofold screws and threefold rotation $C_{3,111}$ satisfy the following relations:

$$[S_{2z}, S_{2y}] = 0, \tag{A4a}$$
$$S_{2z}S_3 = S_3S_{2y}, \tag{A4b}$$
$$S_3S_{2z}S_{2y} = S_{2y}S_3. \tag{A4c}$$

Since S_{2z} and S_{2y} commute, let $|\psi\rangle$ be a simultaneous eigenstate of both S_{2z} and S_{2y} (and also the Hamiltonian since these are the symmetries of the Hamiltonian, i.e., commute with the Hamiltonian by definition).

Let

$$S_{2z}|\psi\rangle = \lambda_1|\psi\rangle, \quad S_{2y}|\psi\rangle = \lambda_2|\psi\rangle, \tag{A5}$$

with $\lambda_1 = \pm 1$, $\lambda_2 = \pm 1$ due to Eqs. (A1) and (A2).

Using the above relations between S_3, S_{2z}, and S_{2y}, we can arrive at

$$\begin{aligned} &S_{2z}S_3|\psi\rangle = S_3S_{2y}|\psi\rangle = \lambda_2S_3|\psi\rangle, \\ &S_{2y}S_3|\psi\rangle = S_3S_{2z}S_{2y}|\psi\rangle = \lambda_1\lambda_2S_3|\psi\rangle, \\ &S_{2z}S^2_3|\psi\rangle = S_3S_{2y}S_3|\psi\rangle = S^2_3S_{2z}S_{2y}|\psi\rangle = \lambda_1\lambda_2S^2_3|\psi\rangle, \\ &S_{2y}S^2_3|\psi\rangle = S_3S_{2z}S_{2y}S_3|\psi\rangle = S^2_3S_{2z}|\psi\rangle = \lambda_1S^2_3|\psi\rangle, \end{aligned} \tag{A6}$$

The set of equations Eqs. (A6) show S_3 generates two new distinct eigenstates $S_3|\psi\rangle$ and $S^2_3|\psi\rangle$ of S_{2z} and S_{2y} provided either $\lambda_1 \neq 1$ or $\lambda_2 \neq 1$. In other words, both screws are nontrivial. These three states will be degenerate since S_3 commutes with the Hamiltonian. Thus, these three states ($|\psi\rangle$, $|S_3\psi\rangle$, $|S^2_3\psi\rangle$) together form a threefold degeneracy at Γ point. The above is a recapitulation of the arguments in Sec. C in the SM of Ref. [3]. The $\lambda_1 = \lambda_2 = 1$ may correspond to a case where both screws are trivial which does not protect any

degeneracy or a case where only one of the screws is trivial which protects only a twofold degeneracy.

b. R point

The generators at the R point are $S_{2x} = \{C_{2x}|\frac{1}{2}, \frac{3}{2}, 0\}$, $S_{2y} = \{C_{2y}|0, \frac{3}{2}, \frac{1}{2}\}$ and $S_3 = \{C_{3,111}^{-1}|0, 1, 0\}$ [37]. They satisfy the following:

$$S_{2x}^2 = -1, \tag{A7a}$$
$$S_{2y}^2 = -1, \tag{A7b}$$
$$S_{2x}S_{2y} = -S_{2y}S_{2x}, \tag{A7c}$$
$$S_{2x}S_3 = S_3S_{2y}, \tag{A7d}$$
$$S_3S_{2x}S_{2y} = S_{2y}S_3. \tag{A7e}$$

The eigenvalues under the twofold screws (S_{2x}, S_{2y}) will be unit modulus and pure imaginary due to Eqs. (A7a) and (A7b). Let $|\psi\rangle$ be an eigenstate of S_{2y} with eigenvalue i without loss of generality, i.e., $S_{2y}|\psi\rangle = i|\psi\rangle$. Then, Eq. (A7c) implies that $|S_{2x}\psi\rangle \equiv S_{2x}|\psi\rangle$ will be an eigenstate of S_{2y} with eigenvalue $-i$ because

$$S_{2y}|S_{2x}\psi\rangle = S_{2y}S_{2x}|\psi\rangle = -S_{2x}S_{2y}|\psi\rangle = -i|S_{2x}\psi\rangle.$$

Since $|\psi\rangle$ and $|S_{2x}\psi\rangle$ have different eigenvalues under S_{2y}, they are orthogonal. Equation (A7d) now implies that $|S_3\psi\rangle \equiv S_3|\psi\rangle$ will be an eigenstate of S_{2x} with eigenvalue i because

$$S_{2x}|S_3\psi\rangle = S_{2x}S_3|\psi\rangle = S_3S_{2y}|\psi\rangle = S_3 i|\psi\rangle = i|S_3\psi\rangle.$$

Equation (A7c) will again imply that $|S_{2y}S_3\psi\rangle \equiv S_{2y}S_3|\psi\rangle$ will be an eigenstate of S_{2x} with eigenvalue $-i$ because

$$S_{2x}|S_{2y}S_3\psi\rangle = S_{2x}S_{2y}|S_3\psi\rangle = -S_{2y}S_{2x}|S_3\psi\rangle = -i|S_{2y}S_3\psi\rangle.$$

Since $|S_3\psi\rangle$ and $|S_{2y}S_3\psi\rangle$ have different eigenvalues under S_{2x}, they are orthogonal [55].

By requiring that S_3 acts nontrivially on the eigenstates of S_{2y} and takes out of the subspace formed by them, we can ensure mutual orthogonality between eigenstates of S_{2y} and S_{2x}. Minimally, $\langle\psi|S_3\psi\rangle = 0$ guarantees all other mutual orthogonalities as follows:

Case of $|S_3\psi\rangle$ and $|S_{2x}\psi\rangle$:

$$\begin{aligned}\langle S_{2x}\psi|S_3\psi\rangle &= \langle\psi|S_{2x}^{-1}S_3|\psi\rangle = \langle\psi|(-S_{2x})S_3|\psi\rangle \\ &= -\langle\psi|S_{2x}S_3|\psi\rangle = \langle\psi|S_3S_{2y}|\psi\rangle \\ &= i\langle\psi|S_3|\psi\rangle = 0.\end{aligned}$$

Case of $|S_{2y}S_3\psi\rangle$ and $|\psi\rangle$:

$$\begin{aligned}\langle\psi|S_{2y}S_3\psi\rangle &= \langle\psi|S_{2y}S_3|\psi\rangle = -\langle\psi|S_{2y}^{-1}S_3|\psi\rangle \\ &= -(-i)\langle\psi|S_3|\psi\rangle = 0.\end{aligned}$$

Case of $|S_{2y}S_3\psi\rangle$ and $|S_{2x}\psi\rangle$:

$$\begin{aligned}\langle S_{2x}\psi|S_{2y}S_3\psi\rangle &= \langle\psi|S_{2x}^{-1}S_{2y}S_3|\psi\rangle \\ &= \langle\psi|(-S_{2x})S_{2y}S_3|\psi\rangle \\ &= -\langle\psi|S_{2x}|S_{2y}S_3\psi\rangle \\ &= i\langle\psi|S_{2y}S_3\psi\rangle = 0.\end{aligned}$$

Therefore, $(|\psi\rangle, |S_{2x}\psi\rangle, |S_3\psi\rangle, |S_{2y}S_3\psi\rangle)$ are four mutually orthogonal states. Thus, we have a symmetry-protected fourfold degeneracy at R point in the absence of spin-orbit coupling.

Since time-reversal squares to identity ($\mathcal{T}^2 = \mathbb{I}$) for spinless fermions, it does not generate any new eigenstates. In fact, it relates the eigenstates of the two screws as follows:

$$\begin{aligned}S_{2y}|\mathcal{T}\psi\rangle = S_{2y}\mathcal{T}|\psi\rangle = \mathcal{T}S_{2y}|\psi\rangle = \mathcal{T}i|\psi\rangle = -i\mathcal{T}|\psi\rangle \\ \Rightarrow S_{2y}|\mathcal{T}\psi\rangle = -i|\mathcal{T}\psi\rangle,\end{aligned}$$

where we have used the facts that $\mathcal{T}$ commutes with the screws, and $\mathcal{T}^\dagger i\mathcal{T} = -i$ (anti-linear property). Thus, we can identify $|\mathcal{T}\psi\rangle$ with $|S_{2x}\psi\rangle$ having same eigenvalue $-i$ under S_{2y}. By a very similar argument, the pairs $\{|\mathcal{T}S_{2x}\psi\rangle, |\psi\rangle\}$, $\{|\mathcal{T}S_3\psi\rangle, |S_{2y}S_3\psi\rangle\}$ and $\{|\mathcal{T}S_{2y}S_3\psi\rangle, |S_3|\psi\rangle\}$ can be identified.

To demonstrate the fourfold degeneracy at the R point for spinless case, we have simulated a few more binary and ternary systems belonging to SG 198. The bulk band structure for these compounds is shown in Fig. S3 of the SM [33]. Similar to CoGe, the electronic structure in all these binary and ternary systems shows the fourfold degeneracy at the R point, irrespective of their location with respect to Fermi level. Thus, the fourfold degeneracy at R point for the spinless case is independent of both the chemical elements at the lattice sites and number of atoms in the cell. Rather, the degeneracy at the R point is strictly determined by the crystal SG symmetry.

3. Spinfull case

The generators at Γ point are $S_{2z} = \{C_{2z}|\frac{1}{2}, 0, \frac{1}{2}\}$, $S_{2y} = \{C_{2y}|0, \frac{1}{2}, \frac{1}{2}\}$ & $S_3 = \{C_{3,111}|0, 0, 0\}$ [37]. They satisfying the following relations for spinfull fermions:

$$S_{2z}^2 = -1, \tag{A8a}$$
$$S_{2y}^2 = -1, \tag{A8b}$$
$$S_3^3 = -1. \tag{A8c}$$

The difference with respect to the corresponding spinless Γ point symmetry relations is due to the different action of $\mathcal{R}$ in these two cases.

Also, we have

$$S_{2z}S_{2y} = -S_{2y}S_{2z}, \tag{A9a}$$
$$S_{2z}S_3 = S_3S_{2y}, \tag{A9b}$$
$$S_3S_{2z}S_{2y} = S_{2y}S_3. \tag{A9c}$$

Therefore, we can use the very same arguments as in Sec. A 2 b to generate a fourfold degeneracy.

Since $\mathcal{T}^2 = -1$ for the spinfull case, it is possible that time reversal may generate further new states. In other words, the question is whether the time-reversed partners of the above fourfold states $\{|\psi\rangle, |S_{2z}\psi\rangle, |S_3\psi\rangle, |S_{2y}S_3\psi\rangle\}$ are distinctly new states or not. As mentioned in the main text, they are actually not new states because mutual orthogonalities are not ensured. This is due to the imaginary eigenvalues under screws.

From $S_{2z}^2 = S_{2y}^2 = \mathcal{T}^2 = -1$, we have $S_{2z}^{-1} = -S_{2z}$, $S_{2y}^{-1} = -S_{2y}$ and $\mathcal{T}^{-1} = -\mathcal{T}$. Also, $\mathcal{T}$ commutes with the screws.

First, these mutual overlaps have to be real, e.g.,

$$\begin{aligned}\langle S_{2z}\psi|\mathcal{T}\psi\rangle &= \langle\psi|S_{2z}^{-1}\mathcal{T}|\psi\rangle = -\langle\psi|S_{2z}\mathcal{T}|\psi\rangle \\ &= -\langle\psi|\mathcal{T}S_{2z}|\psi\rangle = \langle\psi|\mathcal{T}^{-1}S_{2z}|\psi\rangle \\ &= \langle\mathcal{T}\psi|S_{2z}\psi\rangle = \langle S_{2z}\psi|\mathcal{T}\psi\rangle^*.\end{aligned}$$

Second, the eigenvalue of $|\mathcal{T}\psi\rangle$ under S_{2y} is the same as $|S_{2z}\psi\rangle$, and similarly the eigenvalue of $|\mathcal{T}S_{2z}\psi\rangle$ under S_{2y} is the same as $|\psi\rangle$, as follows. Let, $S_{2y}|\psi\rangle = i|\psi\rangle$. Therefore,

$$S_{2y}|S_{2z}\psi\rangle = -i|S_{2z}\psi\rangle$$

by following the same argument as in Sec. A 2 b. Now,

$$\begin{aligned}S_{2y}|\mathcal{T}\psi\rangle &= S_{2y}\mathcal{T}|\psi\rangle = \mathcal{T}S_{2y}|\psi\rangle = \mathcal{T}i|\psi\rangle \\ &= -i\mathcal{T}|\psi\rangle = -i|\mathcal{T}\psi\rangle.\end{aligned}$$

Thus, both $|\mathcal{T}\psi\rangle$ and $|S_{2z}\psi\rangle$ have the same eigenvalues under S_{2y}, and we cannot conclude anything about this mutual orthogonality. The same lack of mutual orthogonality will be the case for the other pairs $\{|\psi\rangle, |\mathcal{T}S_{2z}\psi\rangle\}$, $\{|S_3\psi\rangle, |\mathcal{T}S_{2y}S_3\psi\rangle\}$, and $\{|S_{2y}S_3\psi\rangle, |\mathcal{T}S_3\psi\rangle\}$. Thus, we can at most get a fourfold degeneracy ($\{|\psi\rangle, |S_{2z}\psi\rangle, |S_3\psi\rangle, |S_{2y}S_3\psi\rangle\}$) at Γ point for spinfull fermions in SG 198.

We also note here that for the R point, since now the screws commute and square to 1, the eigenvalues are unit modulus and purely real. We can get a threefold degeneracy ($\{|\psi\rangle, |S_3\psi\rangle, |S_3^2\psi\rangle\}$) by following the same arguments as in Sec. A 2 a. Furthermore, due to eigenvalues being real, the above mutual orthogonalities under time reversal are ensured, and we have three distinctly new time-reversed partners ($\{|\mathcal{T}\psi\rangle, |\mathcal{T}S_3\psi\rangle, |\mathcal{T}S_3^2\psi\rangle\}$). This can give a symmetry-protected sixfold degeneracy at the R spinfull case as discussed in Ref. [3].

4. Twofold degeneracies along R-X and M-X directions

a. Spinless case

The screw rotation along the x axis is $S_{2x} = \{C_{2x}|\frac{1}{2}, \frac{1}{2}, 0\}$. We can define an antiunitary operator $\Theta_{2x} = \mathcal{T}S_{2x}$. $\mathcal{T}$ squares to $+1$ for the spinless case and commutes with the (unitary) screw. Thus we have

$$\begin{aligned}\Theta_{2x}^2 &= \mathcal{T}S_{2x}\mathcal{T}S_{2x} = \mathcal{T}^2S_{2x}^2 \\ &= \mathcal{T}^2\left\{C_{2x}|\frac{1}{2}, \frac{1}{2}, 0\right\}\left\{C_{2x}|\frac{1}{2}, \frac{1}{2}, 0\right\} \\ &= \mathcal{T}^2\left\{C_{2x}^2|C_{2x}\left(\frac{1}{2}, \frac{1}{2}, 0\right) + \left(\frac{1}{2}, \frac{1}{2}, 0\right)\right\} \\ &= \mathcal{T}^2\left\{C_{2x}^2|\left(\frac{1}{2}, \frac{\bar{1}}{2}, 0\right) + \left(\frac{1}{2}, \frac{1}{2}, 0\right)\right\}, \\ &= \mathcal{T}^2\{C_{2x}^2|1, 0, 0\} = \mathcal{T}^2\{\mathcal{R}|1, 0, 0\} \\ &= \{\mathcal{R}|1, 0, 0\} = \{\mathbb{I}|1, 0, 0\} = e^{-ik_x}. \qquad \text{(A10)}\end{aligned}$$

Therefore, on the $k_x = \pi$ plane, $\Theta_{2x}^2 = -1$. Thus, by Kramers argument, if $|\psi\rangle$ is an eigenstate of S_{2x}, then $|\Theta_{2x}\psi\rangle$ is a like a time-reversed partner for $k_x = \pi$. Hence, Θ_{2x} gives a Kramers-like double degeneracy on the $k_x = \pi$ and symmetry-related planes. This in turn implies that the bands along R-X and M-X directions in the BZ are twofold degenerate by the combination of time-reversal and screw symmetry as seen in Fig. 2(a) of the main text.

b. Spinfull case

For the spinfull case, $\mathcal{R} = -\mathbb{I}$ and $\mathcal{T}^2 = -\mathbb{I}$. Therefore, similar to Eq. (A10), it follows that

$$\begin{aligned}\Theta_{2x}^2 &= \mathcal{T}S_{2x}\mathcal{T}S_{2x} = \mathcal{T}^2S_{2x}^2 \\ &= \mathcal{T}^2\{C_{2x}^2|1, 0, 0\} = \mathcal{T}^2\{\mathcal{R}|1, 0, 0\} \\ &= -\mathbb{I}\{-\mathbb{I}|1, 0, 0\} = +e^{-ik_x}.\end{aligned}$$

Thus, similar to the spinless case, $\Theta_{2x}^2 = -1$ again and the bands are doubly degenerate on $k_x = \pi$ and symmetry-related planes even in the spinfull case. These gives the double degeneracy of bands along R-X and M-X and symmetry-related directions in the BZ as also observed in Fig. 2(b) of the main text. We note here that this is again a Kramers-like degeneracy ensured by a combination of time-reversal and screw symmetry on these planes and not the standard Kramers degeneracy which cannot be applied here since inversion symmetry is absent. Screw symmetry is replacing the inversion symmetry on these high-symmetry planes to again make the Kramers argument operational and give us a Kramers-like twofold degeneracy.

[1] S. M. Young, S. Zaheer, J. C. Y. Teo, C. L. Kane, E. J. Mele, and A. M. Rappe, Phys. Rev. Lett. **108**, 140405 (2012).

[2] C. Fang, M. J. Gilbert, X. Dai, and B. A. Bernevig, Phys. Rev. Lett. **108**, 266802 (2012).

[3] B. Bradlyn, J. Cano, Z. Wang, M. G. Vergniory, C. Felser,R. J. Cava, B. Andrei Bernevig, Science **353**, aaf5037 (2016).

[4] P. B. Pal, Am. J. Phys. **79**, 485 (2011).

[5] A. A. Soluyanov, D. Gresch, Z. Wang, QuanSheng Wu, Matthias Troyer, Xi Dai and B. A. Bernevig, Nature **527**, 495 (2015).

[6] N. P. Armitage, E. J. Mele, and A. Vishwanath, Rev. Mod. Phys. **90**, 015001 (2018).

[7] C. K. Barman, C. Mondal, B. Pathak, and A. Alam, Phys. Rev. B **99**, 045144 (2019).

[8] B. J. Wieder, Y. Kim, A. M. Rappe, and C. L. Kane, Phys. Rev. Lett. **116**, 186402 (2016).

[9] C. Mondal, C. K. Barman, A. Alam, and B. Pathak, Phys. Rev. B **99**, 205112 (2019).

[10] B. Q. Lv, Z.-L. Feng, Q.-N. Xu, X. Gao, J.-Z. Ma, L.-Y. Kong, P. Richard, Y.-B. Huang, V. N. Strocov, C. Fang, H.-M. Weng, Y.-G. Shi, T. Qian, and H. Ding, Nature **546**, 627 (2017).

[11] R. Yu, H. Weng, Z. Fang, X. Dai, and X. Hu, Phys. Rev. Lett. **115**, 036807 (2015).

[12] Y. Kim, B. J. Wieder, C. L. Kane, and A. M. Rappe, Phys. Rev. Lett. **115**, 036806 (2015).

[13] J.-T. Wang, H. Weng, S. Nie, Z. Fang, Y. Kawazoe, and C. Chen, Phys. Rev. Lett. **116**, 195501 (2016).

[14] G. Bian, T.-R. Chang, R. Sankar, S.-Y. Xu, H. Zheng, T. Neupert, C.-K. Chiu, S.-M. Huang, G. Chang, I. Belopolski, D. S. Sanchez, M. Neupane, N. Alidoust, C. Liu, BaoKai Wang, C.-C. Lee, H.-T. Jeng, C. Zhang, Z. Yuan, S. Jia, A. Bansil, F. Chou, H. Lin, and M. Zahid Hasan, Nat. Commun. **7**, 10556 (2016).

[15] G. Chang, S.-Y. Xu, B. J. Wieder, D. S. Sanchez, S.-M. Huang, I. Belopolski, T.-R. Chang, S. Zhang, A. Bansil, H. Lin, and M. Zahid Hasan, Phys. Rev. Lett. **119**, 206401 (2017).

[16] H. Miao, T. T. Zhang, L. Wang, D. Meyers, A. H. Said, Y. L. Wang, Y. G. Shi, H. M. Weng, Z. Fang, and M. P. M. Dean, Phys. Rev. Lett. **121**, 035302 (2018).

[17] P. Tang, Q. Zhou, and S.-C. Zhang, Phys. Rev. Lett. **119**, 206402 (2017).

[18] T. Zhang, Z. Song, A. Alexandradinata, H. Weng, C. Fang, L. Lu, and Z. Fang, Phys. Rev. Lett. **120**, 016401 (2018).

[19] The topological charges or Chern numbers being integers cannot change continuously.

[20] D. Takane, Z. Wang, S. Souma, K. Nakayama, T. Nakamura, H. Oinuma, Y. Nakata, H. Iwasawa, C. Cacho, T. Kim, K. Horiba, H. Kumigashira, T. Takahashi, Y. Ando, and T. Sato, Phys. Rev. Lett. **122**, 076402 (2019).

[21] D. S. Sanchez, I. Belopolski, T. A. Cochran, Xitong Xu, J.-X. Yin, G. Chang, W. Xie, K. Manna, V. Süß, C.-Y. Huang, N. Alidoust, D. Multer, S. S. Zhang, N. Shumiya, X. Wang, G.-Q. Wang, T.-R. Chang, C. Felser, S.-Y. Xu, S. Jia, H. Lin, and M. Zahid Hasan, Nature **567**, 500 (2019).

[22] Z. Rao, H. Li, T. Zhang, S. Tian, C. Li, B. Fu, C. Tang, L. Wang, Z. Li, W. Fan, J. Li, Y. Huang, Z. Liu, Y. Long, C. Fang, H. Weng, Y. Shi, H. Lei, Y. Sun, T. Qian, and H. Ding, Nature **567**, 496 (2019).

[23] N. B. M. Schröter, D. Pei, M. G. Vergniory, Y. Sun, K. Manna, F. de Juan, J. A. Krieger, V. Süß, M. Schmidt, P. Dudin, B. Bradlyn, T. K. Kim, T. Schmitt, C. Cacho, C. Felser, V. N. Strocov, and Y. Chen, Nat. Phys. **15**, 759 (2019).

[24] G. Kresse and J. Hafner, Phys. Rev. B **47**, 558(R) (1993)

[25] G. Kresse and D. Joubert, Phys. Rev. B **59**, 1758 (1999)

[26] N. Marzari and D. Vanderbilt, Phys. Rev. B **56**, 12847 (1997).

[27] I. Souza, N. Marzari, and D. Vanderbilt, Phys. Rev. B **65**, 035109 (2001).

[28] N. Marzari, A. A. Mostofi, J. R. Yates, I. Souza, and D. Vanderbilt, Rev. Mod. Phys. **84**, 1419 (2012).

[29] A. A. Mostofi, J. R. Yates, G. Pizzi, Y. S. Lee, I. Souza, D. Vanderbilt, and N. Marzari, Comput. Phys. Commun. **185**, 2309 (2014).

[30] D. H. Lee and J. D. Joannopoulos, Phys. Rev. B **23**, 4988 (1981).

[31] D. H. Lee and J. D. Joannopoulos, Phys. Rev. B **23**, 4997 (1981).

[32] M. P. Lopez Sancho, J. M. Lopez Sancho, J. M. L. Sancho, and J. Rubio, J. Phys. F:Met. Phys. **15**, 851 (1985).

[33] See Supplemental Material at http://link.aps.org/supplemental/10.1103/PhysRevB.102.155147 It contains auxiliary computational details, elaborations on the symmetry arguments presented concisely in the main text, and supplementary evidence from other binary, ternary, and quaternary systems. This includes the Refs. [26–32,34,36,44,56–59].

[34] V. I. Larchev and S. V. Popova, J. Less-Common Met. **87**, 53 (1982).

[35] CoGe exists in SG 198 at ambient pressures as a (metastable) phase once synthesized at high pressures.

[36] L. Wu, J. C. Sun, Y. Zhang, S. F. Jin, Y. F. Kong, and J. J. Xu, Inorg. Chem. **49**, 2715 (2010).

[37] P. Cracknell and Christopher J. Bradley, *The Mathematical Theory of Symmetry in Solids: Representation Theory for Point Groups and Space Groups*, (Oxford: Clarendon Press, 1972).

[38] Basically, the presence of three mutually anticommuting screws in the presence of time-reversal symmetry can not admit twofold (real) representations, only fourfold or higher. (See p. 2, column 2, bottom paragraph in Ref. [18].)

[39] A trivial S_3, i.e., $S_3|\psi\rangle = |\psi\rangle$, is not allowed, since two anticommuting operators cannot share a simultaneous eigenstate with nonzero eigenvalue. S_3 cannot exchange $|\psi\rangle$ and $S_{2x}|\psi\rangle$ as well for the same reason. S_3 can, however, in principle create some linear combination of $|\psi\rangle$ and $S_{2x}|\psi\rangle$, in which case this argument would give a twofold degeneracy.

[40] Verbose details are given in the Appendix.

[41] This difference in screw commutation relations at Γ and R points is due to the different action of a 2π rotation for spinless and spinfull cases.

[42] B. J. Wieder and C. L. Kane, Phys. Rev. B **94**, 155108 (2016).

[43] H. B. Nielsen and M. Ninomiya, Phys. Lett. B **105**, 219 (1981).

[44] N. Audebrand, M. Ellner, and E. J. Mittemeijer, Powder Diffr. **15**, 120 (2000).

[45] Y. Tokura, K. Yasuda, and A. Tsukazaki, Nat. Rev. Phys. **1**, 126 (2019).

[46] S. D. Bader and S. S. P. Parkin, Annu. Rev. Condens. Matter Phys. **1**, 71 (2010).

[47] L. Huang, T. M. McCormick, M. Ochi, Z. Zhao, M.-T. Suzuki, R. Arita, Y. Wu, D. Mou, H. Cao, J. Yan, N. Trivedi, and A. Kaminski, Nat. Mat. **15**, 1155 (2016).

[48] S.-Y. Xu, N. Alidoust, G. Chang, H. Lu, B. Singh, I. Belopolski, D. S. Sanchez, X. Zhang, G. Bian, H. Zheng, M.-A. Husanu, Y. Bian, S.-M. Huang, C.-H. Hsu, T.-R. Chang, H.-T. Jeng, A. Bansil, T. Neupert, V. N. Strocov, H. Lin, S. Jia, and M. Zahid Hasan, Science Advances **3**, e1603266 (2017).

[49] H. Weng, C. Fang, Z. Fang, B. A. Bernevig, and X. Dai, Phys. Rev. X **5**, 011029 (2015).

[50] S.-M. Huang, S.-Y. Xu, I. Belopolski, C.-C. Lee, G. Chang, BaoKai Wang, N. Alidoust, G. Bian, M. Neupane, C. Zhang, S. Jia, A. Bansil, H. Lin, and M. Zahid Hasan, Nat. Commun. **6**, 7373 (2015).

[51] M. Yao, K. Manna, Q. Yang, A. Fedorov, V. Voroshnin, B. V. Schwarze, J. Hornung, S. Chattopadhyay, Z. Sun, S. N. Guin, J. Wosnitza, H. Borrmann, C. Shekhar, N. Kumar, J. Fink, Y. Sun, and C. Felser, Nat. Commun. **11**, 2033 (2020).

[52] M. Armbrüster, H. Borrmann, M. Wedel, Y. Prots, R. Giedigkeit, and P. Gille, Z. Kristallogr. - New Cryst. Struct. **225**, 617 (2010).

[53] D. J. Rebar, S. M. Birnbaum, J. Singleton, M. Khan, J. C. Ball, P. W. Adams, J. Y. Chan, D. P. Young, D. A. Browne, and J. F. DiTusa, Fermi surface, Phys. Rev. B **99**, 094517 (2019).

[54] F. de Juan, A. G. Grushin, T. Morimoto, and J. E. Moore, Nat. Commun. **8**, 15995 (2017).

[55] We also have $S_{2y}S_3 = S_3S_{2x}S_{2y}$ at R point, but this does not give any strong condition about the generation of new states.
[56] P. E. Blöchl, Phys. Rev. B **50**, 17953 (1994).
[57] QuanSheng Wu, ShengNan Zhang, Hai-Feng Song, Matthias Troyer, A. A. Soluyanov, Comp. Phys. Comm. **224**, 405 (2018).
[58] Von E. Schultze-Rhonhof and G. Bergerhoff, Acta Cryst. **B25**, 2645 (1969).
[59] Tatiana A. Shestimerova, Alexander S. Mitiaev, Dmitry I. Davliatshin, and Andrei V. Shevelkov, Z. Anorg. Allg. Chem. **636**, 1941 (2010).